Journal of Alloys and Compounds, 207/208 (1994) 138–145
JALCOM 3007

Neutron spectroscopy in $RBa_2Cu_3O_x$ (R = Ho, Er; $6 < x \leqslant 7$) compounds

A. Furrer, J. Mesot, U. Staub, F. Fauth and M. Guillaume
Laboratory for Neutron Scattering, Eidg. Technische Hochschule Zürich and Paul Scherrer Institut, CH-5232 Villigen PSI (Switzerland)

Abstract

Inelastic neutron scattering has been employed to study the perovskite-type high T_c superconducting compounds $RBa_2Cu_3O_x$ (R = Er, Ho; $6 < x \leqslant 7$). For $ErBa_2Cu_3O_x$, we have determined the crystalline electric field (CEF) level scheme as a function of the oxygen content x. The variation of the energies and intensities of the CEF transitions versus x is shown to be predominantly related to a charge transfer process between the chains and the planes. The observed energy spectra are the result of a superposition of two different metallic components and a semiconducting one, *i.e.* there is clear experimental evidence for phase separation. A two-dimensional bond percolation model explains the appearance of superconductivity as well as the critical oxygen concentrations associated with the two-plateau structure of T_c. For $HoBa_2Cu_3O_7$, we have measured the low-lying magnetic excitations of Ho^{3+} ions in a grain-aligned sample. From the dispersive behavior of the spin-wave excitations, we derive the nearest-neighbor magnetic coupling parameters in the Heisenberg approximation. From complimentary experiments on a magnetically diluted $Ho_{0.1}Y_{0.9}Ba_2Cu_3O_7$ compound, we have been able to observe Ho^{3+} dimer excitations which allow a direct determination of the magnetic coupling strength in the (a,b) plane. The line shapes of the Ho^{3+} excitations turn out to be highly asymmetric which we interpret in terms of an exchange interaction between the Ho^{3+} spins and the fluctuating Cu^{2+} spins.

1. Introduction

The discovery of high T_c superconductivity in the perovskite-type copper oxide compounds has given rise to a large amount of materials research. Of particular interest in determining the nature of the superconductivity is the effect of substituents at various sites in these compounds. It has been realized that the superconducting transition temperature is essentially unchanged upon replacing the Y and La ions by "magnetic" rare earth (R) ions. This surprising observation is in contrast to conventional superconductors, for which paramagnetic ions usually have a large detrimental effect on superconductivity. It is therefore important to achieve a detailed understanding of the low energy electronic properties which define the magnetic ground state of the R ions. In particular, information on the crystalline electric field (CEF) interaction at the R site is highly desirable, for the following reasons:

(i) For many high T_c compounds, superconductivity and long-range three-dimensional magnetic ordering of the R ion sublattice co-exist at low temperatures. An understanding of both the nature of the magnetic ordering and its apparent lack of influence on T_c requires a detailed knowledge of the CEF states of the R ions.

(ii) In most high T_c compounds, the R ions are situated close to the CuO_2 planes where it is widely believed that the superconducting carriers are located, thus the CEF interaction at the R site constitutes an ideal probe of both the local symmetry and the charge distribution of the superconducting planes and thereby monitors directly changes of the carrier concentration induced, *e.g.* by oxygen non-stoichiometry, pressure and disordering effects.

(iii) The temperature dependence of the linewidth of CEF excitations provides information on the superconducting energy gap.

Very detailed and direct information about the CEF interaction results from inelastic neutron scattering (INS) experiments, particularly for optically opaque materials like the high T_c compounds. There has been considerable effort made to study the CEF interaction in these systems by the INS technique, and a complete quantitative understanding of the CEF level structure has been obtained for a large number of high T_c compounds of type $RBa_2Cu_3O_6$, $RBa_2Cu_3O_7$, $RBa_2Cu_4O_8$, $R_{2-x}Ce_xCuO_4$, and $Bi_2Sr_2Ca_{1-x}R_xCu_2O_8$ by various groups working at the neutron sources in Argonne (IPNS-ANL), Didcot (ISIS-RAL), Gaithersburg (CNRF-NIST), Grenoble (HFR-ILL), and Würenlingen (Saphir-PSI) [1–5]. In addition, changes in

0925-8388/94/$07.00
SSDI 0925-8388(93)03007-6

the CEF interaction induced by oxygen non-stoichiometry, pressure, and doping at the copper sites have been studied in detail [6]. INS measurements of the temperature dependence of inelastic CEF transitions have brought important information about the opening of the energy gap [7].

Of equal importance towards understanding the interplay of magnetism and superconductivity in the perovskite-type copper oxide compounds is the knowledge of the coupling mechanism between the R^{3+} ions. As recently discussed by Misra and Felsteiner [8], several mechanisms could be involved in the coupling of the R^{3+} ions to form two- or three-dimensional spin structures: dipolar, Ruderman–Kitte–Kasuya–Yosida (RKKY) and superexchange interactions. Calculations based on dipolar interactions alone result in Néel temperatures which are much lower than the observed ordering temperatures, and there are controversies as to the importance of either RKKY or superexchange interactions. Some qualitative information on the coupling of the R^{3+} ions has been obtained from magnetization and low temperature specific heat measurements which indicate large anisotropies of the exchange interaction in the (a,b)-plane [9]. A more detailed insight into the coupling mechanism results from studying the spin dynamics through the measurement of the collective magnetic excitations or spin waves which inherently contain information on the nature and size of the magnetic coupling between the R^{3+} ions. Again, the INS technique provides the most direct access to this property and thereby allows a very direct determination of exchange parameters; however, so far, INS measurements have only been performed for a grain-aligned sample of $HoBa_2Cu_3O_7$ [10].

In this review, we present neutron spectroscopic data obtained for $RBa_2Cu_3O_x$ (R = Er, Ho; $6 < x \leqslant 7$). In $ErBa_2Cu_3O_x$, the CEF interaction splits the ground state J multiplet $^4I_{15/2}$ of the Er^{3+} ions into eight Kramers doublets Γ_n. We have been able to resolve the seven ground state transitions for a series of samples covering the superconducting phase as well as the semiconducting one [11]. J-mixing and intermediate coupling effects as well as geometrical considerations are necessary to determine the CEF parameters unambiguously. The large energy shifts and intensity changes of the observed CEF spectra as a function of the oxygen content x are shown to be related predominantly to a charge transfer process between the chains and the planes. The observed energy spectra are found to be the result of a superposition of three stable states, which we interpret in terms of local regions of semiconducting and metallic character, *i.e.* there is clear experimental evidence for phase separation. The superconductivity is shown to result from the formation of a two-dimensional percolative network. A two-dimensional bond percolation model correctly predicts the critical oxygen content associated with the two-plateau structure of T_c [12]. For $HoBa_2Cu_3O_x$, the low-lying CEF excitations exhibit significant dispersion effects from which we derive information on the magnetic coupling parameters [10]. The results are compatible with a methodologically different experiment on a magnetically diluted $Ho_{0.1}Y_{0.9}Ba_2Cu_3O_7$ compound which allows the direct determination of the magnetic coupling strength of Ho^{3+} pairs in the (a,b)-plane through the observation of Ho^{3+} dimer excitations. The observed line shapes turn out to be highly asymmetric and can be modelled by an exchange interaction between the Ho^{3+} spins and the fluctuating Cu^{2+} spins. Our results strongly support the magnetic polaron picture in the understanding of high T_c superconductivity in perovskites [13].

2. Crystal field excitations in $ErBa_2Cu_3O_x$ ($6 < x < 7$)

The energy spectra observed for $ErBa_2Cu_3O_x$ at $T = 10$ K exhibit seven inelastic lines which are considerably separated in energy: we observe three inelastic lines A, B, C in a low energy window ($\Delta E < 12$ meV) and four inelastic lines D, E, F, G in a high energy window ($65 < \Delta E < 82$ meV) as shown in Fig. 1. The gap between the two windows is structureless. A detailed analysis of the temperature and momentum transfer

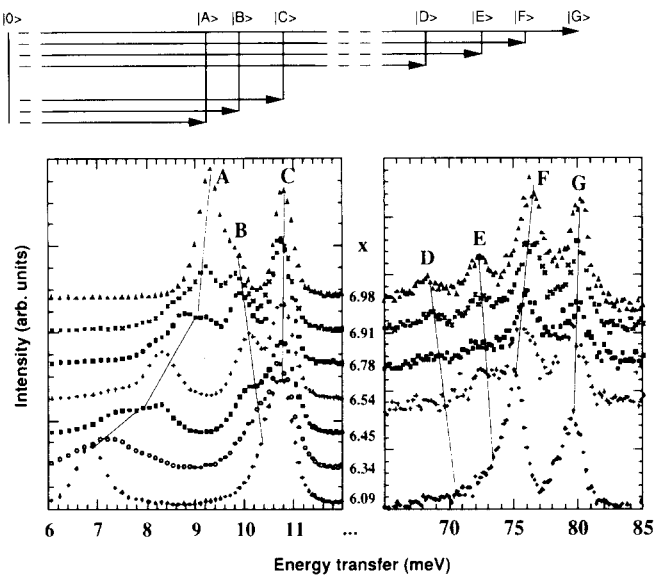

Fig. 1. Energy spectra of neutrons scattered from $ErBa_2Cu_3O_x$ at $T = 10$ K, measured with use of the time-of-flight spectrometers IN4 (left part, $E_i = 17.2$ meV) and HET (right part, $E_i = 100$ meV) installed at the Institute Laue-Langevin, Grenoble, and at the Rutherford Appleton Laboratory, Chilton, respectively. The lines indicate the x dependence of the observed ground state CEF transitions. The top of the figure shows the resulting CEF level scheme for $x = 6.98$.

dependence of these transitions allows us to interpret all seven lines in terms of CEF excitations out of the ground state. Thus, the CEF level structure is completely determined.

Upon oxygen increase, the transitions B, D, E shift slightly to lower energies, and the transitions A, F, G move up to higher energies, whereas the energy of the transition C remains unchanged (see Fig. 1). Note that the linewidth of the transitions B–G is a monotonic function of x, in contrast to the linewidth of the transition A which shows a highly unusual behavior; it is rather narrow for $x=6.98$, $x=6.53$ and $x=6.09$, but for the other concentrations x, it is considerably broadened and even exhibits substructures. These unusual features are discussed in detail in Section 3.

We base the analysis of the observed energy spectra on the CEF Hamiltonian

$$H_{\mathrm{CEF}}=\sum_{n=1}^{3}\sum_{m=0}^{n} A_{2n}^{2m}(Y_{2n}^{2m}+Y_{2n}^{-2m}) \tag{1}$$

where A_{2n}^{2m} denote the CEF parameters and Y_{2n}^{2m} are spherical tensor operators [14]. The center of gravity and the integrated intensity of each of the seven observed ground state transitions A–G have been considered for the fitting of the CEF parameters. Although this is sufficient to determine unequivocally all five CEF parameters of the tetragonal phase, some more information is needed to achieve a unique determination of the nine orthorhombic CEF parameters. In order to solve this problem, we first imposed strict conditions based on geometrical relations determined by the nearest-neighboring oxygen shell [5,11]. In a second step, we progressively released the constraints until all parameters were simultaneously refined. We then used the final parameters of the $x=6.09$ and $x=6.98$ samples as starting values for the other oxygen concentrations.

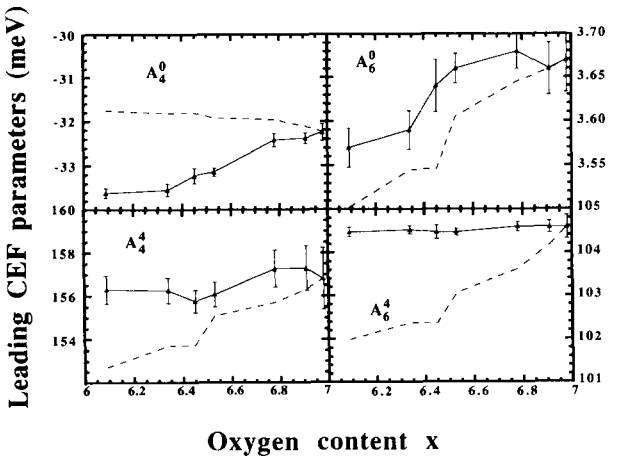

Fig. 2. Leading fourth- and sixth-order CEF parameters determined for $ErBa_2Cu_3O_x$ in the present work (triangles and solid curves). The values extrapolated from the structural changes alone are indicated by the dashed curves.

The final result did not depend on whether we started from the high or the low oxygen concentration parameters, which proves that we arrived at the correct set of parameters. Moreover, the reliability of the CEF parameters was checked by calculating some thermodynamic magnetic properties of $ErBa_2Cu_3O_x$ which were found to be in remarkable agreement with the experimental data [11]. The leading CEF parameters are displayed in Fig. 2.

3. Charge transfer, phase separation, and percolative superconductivity in $ErBa_2Cu_3O_x$

The CEF parameters are related by definition to both the structural arrangement and the charge distribution of the ligand ions. In the basic definition of the CEF potential,

$$V_{\mathrm{CEF}}(\mathbf{r})=\int \rho(\mathbf{R}_i)/|\mathbf{r}-\mathbf{R}_i|\,\mathrm{d}\mathbf{R}_i \tag{2}$$

where $\rho(\mathbf{R}_i)$ denotes the charge distribution at the ligand site $\mathbf{R}_i$ ($\rho(\mathbf{R}_i)=Z_i e|e|$ in the point-charge approximation), the structure and charge aspects are decoupled, so that we can differentiate between them by writing the CEF parameters in the form

$$A_{2n}^{2m}=e|e|\langle r^{2n}\rangle\sum_i Z_i\gamma_{2n}^{2m}(\mathbf{R}_i) \tag{3}$$

Here, $\langle r^{2n}\rangle$ is the $2n$th moment of the distribution of the 4f electrons, Z_i is the charge of the ligand ion at site $\mathbf{R}_i$ in units of the electron charge $|e|$ and $\gamma_{2n}^{2m}(\mathbf{R}_i)$ are geometrical coordination factors as defined, *e.g.* by Hutchings [15]. Restricting to the nearest-neighboring oxygen coordination shell for the definition of $\gamma_{2n}^{2m}(\mathbf{R}_i)$ in eqn. (3), we found that structural considerations alone are not sufficient to reproduce the observed variation of the CEF parameters versus the oxygen content x. As an example, the modulus of the CEF parameter A_4^0 increases upon oxygen reduction, while the structure expands. An increase of the plane-oxygen charge, however, can reproduce the experimental findings. This is consistent with the mechanism of electronic charge transfer from the chains to the planes [16]. A quantitative analysis [11] yields a charge transfer of $0.07|e|$/O when going from $x=6$ to $x=7$ (see Fig. 3), which means that about 28% of the created holes go into the planes. This is slightly less than the value of 40% derived from resistivity measurements [17] and slightly more than the charge transfer 0.04 $|e|$/O (0.08$|e|$/Cu) derived from diffraction data by means of the bond valence sum formalism [16] for the related $YBa_2Cu_3O_x$ compound. Our results suggest a linear dependence of the charge transferred as a function of x, in contrast to Cava *et al.* [16] who deduced a close relation between the two-plateau structure of T_c and the charge transfer

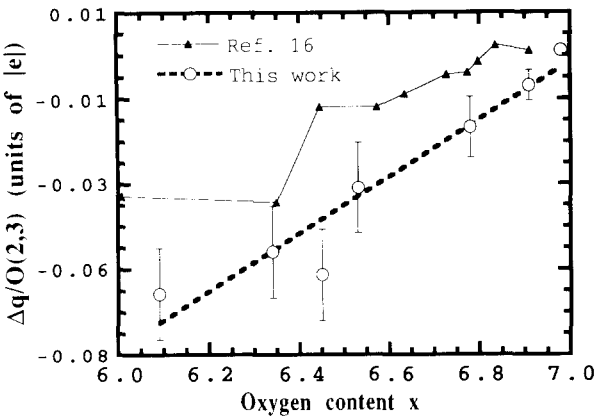

Fig. 3. Charge transfer versus oxygen content x derived for $ErBa_2Cu_3O_x$ in the present work, in comparison with the results obtained for $YBa_2Cu_3O_x$ from bond valence sum considerations (ref. 16).

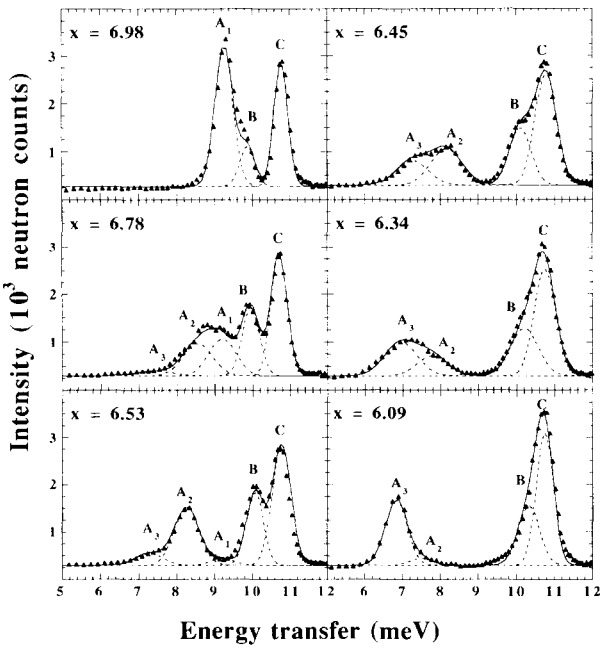

Fig. 4. Low energy part of the neutron spectra observed for $ErBa_2Cu_3O_x$ at $T = 10$ K. The lines are the result of a decomposition into individual Gaussian peaks as explained in detail in ref. 12.

with a pronounced discontinuity at $x \approx 6.4$. In the bond valence sum formalism, a (non-)linear charge transfer is a direct consequence of a (non-)linear decrease in the cell parameter c with increasing x. In this respect, the data by Cava *et al.* [16] are at variance with recent diffraction work published by Radaelli *et al.* [18] who observed a linear relation between the lattice parameter c and the oxygen concentration x for $ErBa_2Cu_3O_x$ ($6 < x < 7$), which nicely supports the results of our CEF analysis.

As mentioned in Section 2 and shown in Fig. 4, there is evidence for substructures associated with the CEF transition A. More specifically, the CEF transition A appears to be decomposed into three individual transitions A_1, A_2 and A_3 as indicated by the dashed lines in Fig. 4. The main characteristics can be summarized as follows:

(i) *Intensities*: The transitions A_1, A_2 and A_3 have maximum weight close to $x = 7.0$, $x = 6.5$ and $x = 6.0$, respectively. With the CEF interaction being a local probe, there is no doubt that the above substructures originate from different local environments of the Er^{3+} ions which obviously co-exist in the compound $ErBa_2Cu_3O_x$.

(ii) *Energies*: Whereas all the CEF transitions are independent of energy for oxygen contents $x > 6.5$, within the experimental error, they shift slightly when going from $x \approx 6.5$ to $x \approx 6.0$. This may be due to the structural discontinuities at the orthorhombic to tetragonal phase transition at $x \approx 6.4$.

(iii) *Linewidths*: The intrinsic linewidths of the transitions A_i are much smaller for oxygen contents where these transitions individually reach their maximum weight, namely for $x \approx 6.0$, 6.5 and 7.0. The linewidths obviously reflect the structural homogeneity around the Er^{3+} ions which is well defined when only one particular cluster type dominates. The rather high degree of homogeneity around $x \approx 6.5$ may also be related to superlattice ordering of the CuO chains.

These findings provide clear experimental evidence for cluster formation or phase separation. It is tempting to identify the three clusters associated with the transition A_1, A_2 and A_3 by two local regions of metallic ($T_c \approx 90$ K, $T_c \approx 60$ K) and a local region of semiconducting character, respectively. Figure 5 shows the fractional proportions of the three cluster types which correspond to the observed intensities of the transitions A_i corrected by the corresponding matrix element. They exhibit a continuous behavior versus the oxygen content x, consistent with our earlier findings that the transfer of holes into the CuO_2 planes is linearly related to the oxygenation process. The continuous increase in the metallic states A_1 and A_2 can also explain the increase in the superconducting volume fraction as observed by magnetic susceptibility measurements [18] when the oxygen content is raised from $x = 6$ to $x = 7$.

Our current understanding of the superconducting properties of $ErBa_2Cu_3O_x$ (and more generally all the $RBa_2Cu_3O_x$ compounds) involves a percolation mechanism of electric conductivity as recently discussed in both theoretical [19] and experimental [20] work. For $x = 6$, the system is a perfect semiconductor. When adding oxygen ions into the chains, holes are continuously transferred into the CuO_2 planes [6,11]. By this mechanism, the number of local regions with metallic character (associated with the CEF transition A_2) rises, which can partially combine to form larger regions. For

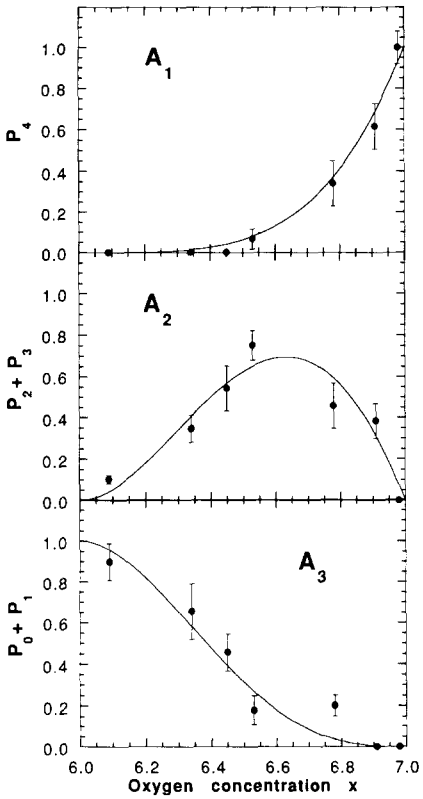

Fig. 5. Proportions of the lowest-lying CEF transitions A_i of $ErBa_2Cu_3O_x$ as a function of the oxygen content x. The lines refer to geometrical probability functions as explained in the text.

some critical concentration, a percolative network is built up, and the system undergoes a transition from the semiconducting to the conducting state (with $T_c \approx 60$ K). Upon further increasing the hole concentration, a second (different) type of metallic cluster (associated with the CEF transition A_1) is formed which start to attach to each other and at the percolation limit induce a transition into another conducting state (with $T_c \approx 90$ K). For a two-dimensional square structure, the critical concentration for bond percolation is $p_c = 50\%$ [21]. From the fractional proportions of A_2 and A_1 displayed in Fig. 5, we can then immediately determine the critical oxygen concentrations for the transitions from the semiconducting to the $T_c \approx 60$ K superconducting state and to the $T_c \approx 90$ K superconducting state to be $x_2 = 6.42$ and $x_1 = 6.86$, respectively, which is in excellent agreement with the observed two-plateau structure of T_c [16,22]. For three-dimensional structures, on the other hand, the critical concentration for bond percolation is 20% (face-centered cubic) $< p_c <$ 30% (simple cubic) [21]. From Fig. 5, we derive $6.21 < x_2 < 6.31$ and $6.64 < x_1 < 6.73$, which is inconsistent with the observed two-plateau structure of T_c. This reinforces the well known fact that the superconductivity in the perovskite-type compounds has indeed a two-dimensional character.

Combined statistical and geometrical considerations may be useful to understand the x-dependent profiles of the fractional proportions of the three cluster types visualized in Fig. 5. In an earlier publication [23], we have developed a local symmetry model and defined the following probabilities $P_k(y)$, for a given oxygen content $x = 6+y$, k of the four oxygen chain sites (0,1/2,0), (1,1/2,0), (0,1/2,1) and (1,1/2,1) nearest to the Er^{3+} ion occupied:

$$P_k(y) = \binom{4}{k} y^k (1-y)^{4-k} \qquad (0 \leqslant k \leqslant 4) \tag{4}$$

The fractional proportion of the cluster type A_1 exhibits the behavior predicted by the probability function $P_4(y)$ (*i.e.* all the oxygen chain sites occupied). Similarly, the fractional proportions of the cluster types A_2 and A_3 follow the sum of the probability functions $P_3(y)+P_2(y)$ (*i.e.* one or two empty oxygen chain sites) and $P_1(y)+P_0(y)$ (*i.e.* one or no oxygen chain site occupied), respectively. The above probability functions are shown in Fig. 5 by solid lines which excellently reproduce the experimental data.

4. Exchange interaction in $HoBa_2Cu_3O_7$

We have chosen $HoBa_2Cu_3O_7$ to study the magnetic coupling within the rare earth sublattice for three specific reasons. Firstly, a recent low temperature neutron diffraction study [24] of $HoBa_2Cu_3O_7$ indicates the existence of three-dimensional correlations associated with the Ho^{3+} sublattice below $T_N \approx 0.19$ K, as well as a three-dimensional or mean-field-type behavior of the zero-field magnetization with a critical exponent $\beta = 0.4 \pm 0.1$, so that we may expect the magnetic excitations to exhibit dispersion effects (contrary to some other $RBa_2Cu_3O_7$ systems with essentially two-dimensional Ising character, *i.e.* $\beta = 0.125$). Secondly, a recent theoretical analysis of the low temperature ordered states of $RBa_2Cu_3O_7$ [8] revealed the importance of exchange interactions for R = Ho. Thirdly, and most importantly, the CEF level scheme of $HoBa_2Cu_3O_7$ is characterized by a series of low-lying states [5] which can be sufficiently resolved within the small range of energy dispersion anticipated for these systems.

We have studied in great detail the dispersive behavior of the low-lying magnetic excitations associated with the Ho^{3+} sublattice in a grain-aligned sample. Preliminary results have been published in ref. 10. Here we present new experimental data taken under improved energy resolution. A polycrystalline $HoBa_2Cu_3O_7$ sample of 1 cm^3 volume was grain-aligned under the action of an external field $H = 5$ T. This procedure resulted in an alignment of the grains along the z-axis, whereas the x- and y-axes remained randomly oriented. Our

INS experiments covered a large region of reciprocal space for scattering vectors $\mathbf{Q}=2\pi(x'/a,\ z/c)$ with $x'=\sqrt{(x^2+y^2)}$ (assuming $a=b$). The ground state CEF excitation $\Gamma_3\rightarrow\Gamma_4$ showed up as a well resolved inelastic line as exemplified in Fig. 6. The energy of maximum peak intensity of this excitation varies considerably when following $\mathbf{Q}$ along the x'-axis, whereas it remains more or less constant upon variation of $\mathbf{Q}$ along the z-axis. In the random phase approximation [25], the excitation energies are given by

$$\hbar\omega(\mathbf{Q})=\left[\Delta\left\{\Delta-4M^2J(\mathbf{Q})\ \mathrm{tgh}\left(\frac{\Delta}{2k_BT}\right)\right\}\right]^{1/2} \tag{5}$$

Here, Δ corresponds to the energy separation between the CEF ground state Γ_3 and the first excited CEF state Γ_4, and M is the dipole transition matrix element between the two CEF states [5]. For the calculation of $J(\mathbf{Q})$, we took into account Heisenberg-type exchange parameters J_a, J_b and J_c, coupling the central Ho^{3+} ion pairwise with the Ho^{3+} ions at the nearest-neighbor positions $\pm a$, $\pm b$, and $\pm c$ along the x-, y- and z-directions, respectively. From the absence of dispersion along the z-axis, we immediately conclude that

$$J_c=0\pm0.2\ \mu\mathrm{eV}$$

as actually expected from the large separation of the Ho^{3+} ions along that axis. Information on J_a and J_b is more difficult to obtain because of the random orientation of the x- and y-axes in our sample, thus the magnetic excitation spectra cannot be analysed directly according to eqn. (5), but we have to average eqn. (5) in the (x,y)-plane as discussed in detail in ref. 10. We obtained

$$J_a=0.5\pm0.1\ \mu\mathrm{eV}$$

$$J_b=-1.6\pm0.2\ \mu\mathrm{eV}$$

Thus, our data analysis resulted in an enormous spatial anisotropy of the magnetic coupling parameters, which are weakly ferromagnetic, antiferromagnetic and almost zero for nearest-neighbour Ho^{3+} pairs along the a-, b- and c-axes, respectively, which nicely confirms the particular type of long-range magnetic ordering recently established for $HoBa_2Cu_3O_7$ [24].

In a methodologically different approach, we have also investigated the magnetic excitations in the diluted compound $Ho_{0.1}Y_{0.9}Ba_2Cu_3O_7$, which according to statistics contains 66% monomers, 29% dimers, and less than 5% trimers, tetramers, etc. of Ho^{3+} ions. The spectral response of Ho^{3+} monomers corresponds to the CEF energy level sequence which has been established in detail [5]. The magnetic coupling of the Ho^{3+} ions in the dimers produces a splitting of the CEF states. Trimers, tetramers, etc. will produce a more complicated splitting pattern, however we can neglect them in the present investigation due to their small statistical probability. We therefore assume the energy spectrum of $Ho_{0.1}Y_{0.9}Ba_2Cu_3O_7$ to be a superposition of CEF transitions (due to Ho^{3+} monomers) and pair transitions (*i.e.* split CEF transitions due to Ho^{3+} dimers). Figure 7 shows that our expectations are clearly supported by the experimental data. The energy splitting associated with the pair transitions amounts to about 0.15 meV which is directly related to the nearest-neighbor Ho^{3+} coupling. A detailed calculation based on the dimer spin Hamiltonian

$$\hat{H}_d=\hat{H}_{\mathrm{CEF}}(1)+\hat{H}_{\mathrm{CEF}}(2)-2J\hat{\mathbf{S}}_1\cdot\hat{\mathbf{S}}_2 \tag{6}$$

yields [26]

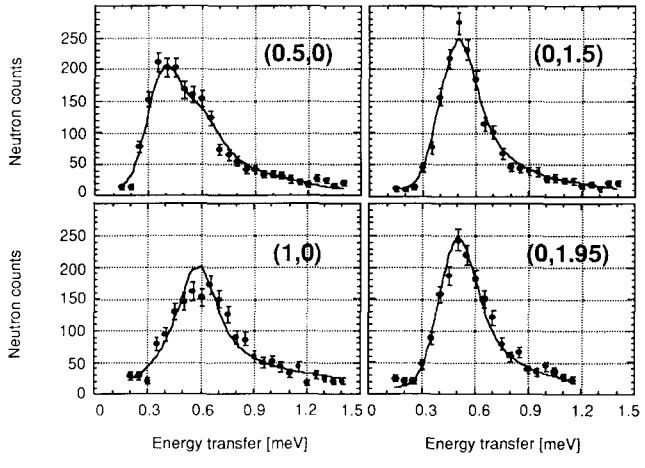

Fig. 6. Energy spectra of neutrons scattered from grain-aligned $HoBa_2Cu_3O_7$ at $T=1.5$ K for different scattering vectors $\mathbf{Q}=2\pi(x/a,\ y/b,\ z/c)$ abbreviated by (x',z) with $x'=\sqrt{(x^2+y^2)}$ (assuming $a=b$), measured with use of the triple-axis spectrometer V2 at the Hahn-Meitner-Institut, Berlin. The lines are the results of a least-squares fitting procedure as discussed in the text.

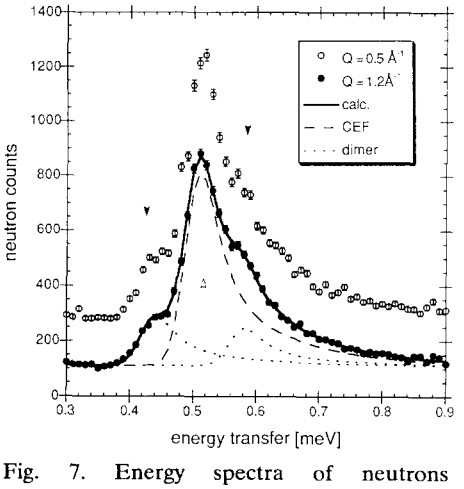

Fig. 7. Energy spectra of neutrons scattered from $Ho_{0.1}Y_{0.9}Ba_2Cu_3O_7$ at $T=1.5$ K, measured with use of the high resolution spectrometer IRIS at the Rutherford Appleton Laboratory, Chilton. The background for the low Q data is enhanced by 200 neutron counts.

$J_a = -J_b = 1.3 \pm 0.2$ μeV

From these values we calculate the molecular field parameter to be $\lambda = 5.2 \pm 0.8$ μeV, which is in good agreement with $\lambda = 5.6$ μeV derived by fitting the zero-field magnetization data [24]. The analysis of the data for grain-aligned $HoBa_2Cu_3O_7$ clearly underestimated the ferromagnetic coupling ($J_a = 0.5 \pm 0.1$ μeV), but gave a reasonable value for the antiferromagnetic coupling ($J_b = -1.6 \pm 0.2$ μeV).

A characteristic of the observed spectra displayed in Figs. 6 and 7 is the asymmetric line shape with a pronounced tail on the high energy side. An anomalous line shape of CEF transitions has already been observed in the very first neutron scattering experiments on $HoBa_2Cu_3O_x$ [5]. At that time, the conjecture was made that this effect is most likely due to local distortions of the charge distribution caused by the oxygen vacancy concentration x. This idea has recently been confirmed for $ErBa_2Cu_3O_x$ through the observed co-existence of different types of local regions whose spectral weights distinctly depend on the oxygen content x (see Section 3). For the presently studied fully oxygenated compounds $HoBa_2Cu_3O_7$ and $Ho_{0.1}Y_{0.9}Ba_2Cu_3O_7$, however, this explanation does not hold. An obvious modelling mechanism for the line shape is then the exchange interaction between the Ho^{3+} spins and the fluctuating Cu^{2+} spins in the superconducting CuO_2 planes. We have treated the Cu^{2+} spin fluctuations in the dynamic effective field approximation [27] which indeed produces a line shape compatible with the experimental findings (see Figs. 6 and 7). The variance of the (Gaussian) probability distribution for the fluctuating field, left free as a fitting parameter in the least-squares procedure, turned out to be of the order of 1 T, which nicely confirms the results obtained by EPR measurements in aligned powders of $Y_{0.99}R_{0.01}Ba_2Cu_3O_{6.85}$ (R = Er,Yb) [28].

5. Concluding remarks

We emphasize the role of neutron spectroscopy among all experimental techniques as a unique and powerful tool to determine the CEF interaction in the low symmetry high T_c compounds. Any attempts to unravel the CEF level structure from the bulk properties are likely to fail because of the complexity of the CEF interaction in these systems. The CEF parameters derived from INS studies on high T_c compounds essentially reflect the charge distribution in the superconducting CuO_2 planes. The changes in the CEF parameters versus oxygen deficiency observed for the "123" compounds can then be interpreted in terms of charge redistribution in the CuO_2 planes, *i.e.* the concept of electronic charge transfer between the chains and the planes is confirmed in a very direct way. The same kind of results presented in Section 3 for $ErBa_2Cu_3O_x$ have also been observed for $HoBa_2Cu_3O_x$ by neutron CEF spectroscopy [29].

In addition, neutron spectroscopy reveals phase separation effects in these compounds which cannot be studied for example by diffraction measurements due to the rather small localization range anticipated for the different clusters. Indeed, a recently proposed ferromagnetic cluster model [19] predicts the local phases in $La_{2-x}(Ba,Sr)_xCuO_4$ and $RBa_2Cu_3O_x$ compounds to include thirteen and five plane copper ions, respectively, *i.e.* the localization range is restricted to a few unit cells only. While the semiconducting to metal transition may also be understood and related to the recently reported phase separation effects at $x \approx 6.4$ [18], the co-existence of two different metallic clusters can only be detected by local probes such as neutron CEF spectroscopy as outlined in the present work.

The INS technique is also a unique tool towards the determination of the magnetic coupling strength associated with the rare earth sublattice as demonstrated by the observation of both dispersion effects for grain-aligned $HoBa_2Cu_3O_7$ and Ho^{3+} dimer excitations in magnetically diluted $Ho_{0.1}Y_{0.9}Ba_2Cu_3O_7$. For these compounds, we observe a strong magnetic anisotropy in the (a,b)-plane which cannot be reproduced either by dipolar or by RKKY interactions, thus the coupling of the Ho^{3+} ions is presumably dominated by nearest-neighbor superexchange interactions mediated by the O(2) and O(3) ions as oxygen bridges, which – at the same time – also take part in the superconducting processes. The charge distribution at the plane oxygen sites is therefore one of the most crucial quantities towards a detailed understanding of the relevant physical properties of the $RBa_2Cu_3O_7$ compounds. The observation of highly asymmetric line shapes of the Ho^{3+} excitations is another feature of current interest. Our interpretation in terms of fluctuating magnetic fields at the Ho^{3+} sites due to plane copper spin fluctuations is consistent, *e.g.* with the magnetic polaron model of high T_c superconductivity in perovskites [13,19] which predicts the occurrence of hole-induced ferromagnetic clusters (ferrons) in the CuO_2 planes.

Acknowledgment

Financial support by the Swiss National Science Foundation is gratefully acknowledged. We are thankful to C.J. Carlile, H. Mutka, R. Osborn, A. Taylor and P. Vorderwisch for their collaboration in part of the experiments as well as to P. Dosanjh and H. Zhou for

the preparation of the grain-aligned $HoBa_2Cu_3O_7$ sample.

References

1 L. Soderholm, C.K. Loong, G.L. Goodman and B.D. Dabrowski, *Phys. Rev. B, 43* (1991) 7923.
2 A.T. Boothroyd, S.M. Doyle, D. McK. Paul and R. Osborn, *Phys. Rev. B, 45* (1992) 10075.
3 A.I. Goldman, Y. Gao, S.T. Ting, J.E. Crow, W.H. Li and J.W. Lynn, *J. Magn. Magn. Mater., 76–77* (1988) 607.
4 U. Staub, P. Allenspach, J. Mesot, A. Furrer, R. Müller, T. Schweizer, L.J. Gaukler, H. Blank and H. Mutka, *Z. Phys. B: Condensed Matter, 85* (1991) 35.
5 A. Furrer, P. Brüesch and P. Unternährer, *Phys. Rev. B, 38* (1988) 4616.
6 A. Furrer, P. Allenspach, J. Mesot, U. Staub, H. Blank, H. Mutka, C. Vettier, E. Kaldis, J. Karpinski, S. Rusiecki and A. Mirmelstein, *Eur. J. Solid State Inorg. Chem., 28* (1991) 627.
7 E.A. Goremychkin, R. Osborn and A.D. Taylor, *JETP Lett., 50* (1989) 380.
8 S.K. Misra and J. Felsteiner, *Phys. Rev. B, 46* (1992) 11033.
9 K.N. Yang, J.M. Ferreira, B.W. Lee, M.B. Maple, H.W. Li, J.W. Lynn and R.W. Erwin, *Phys. Rev B, 40* (1989) 10963.
10 U. Staub, F. Fauth, M. Guillaume, J. Mesot, A. Furrer, P. Dosanjh and H. Zhou, *Europhys. Lett., 21* (1993) 845 (in this paper, the prefactor 2 was omitted in the definition of the Heisenberg Hamiltonian).
11 J. Mesot, P. Allenspach, U. Staub, A. Furrer, H. Mutka, R. Osborn and A. Taylor, *Phys. Rev. B, 47* (1993) 6027.
12 J. Mesot, P. Allenspach, U. Staub, A. Furrer and H. Mutka, *Phys. Rev. Lett., 70* (1993) 865.
13 V. Hizhnyakov and E. Sigmund, *Physica C, 156* (1988) 655.
14 B.R. Judd, *Operator Techniques in Atomic Spectroscopy*, McGraw-Hill, New York, 1963.
15 M.T. Hutchings, in F. Seitz and D. Turnbull (eds.), *Solid State Physics*, Vol. 16, Academic Press, New York, 1964, p. 227.
16 R.J. Cava, A.W. Hewat, E.A. Hewat, B. Battlog, M. Marezio, K.M. Rabe, J.J. Krajewski, W.F. Peck, Jr. and L.W. Rupp, Jr., *Physica C, 165* (1990) 419.
17 U. Welp, S. Flescher, W.K. Kwok, J. Downey, Y. Fang, G.W. Crabtree and J.Z. Liu, *Phys. Rev. B, 42* (1990) 10189.
18 P.G. Radaelli, C.U. Segre, D.G. Hinks and J.D. Jorgensen, *Phys. Rev. B, 45* (1992) 4923.
19 V. Hizhnyakov, N. Kristoffel and E. Sigmund, *Physica C, 160* (1989) 119.
20 R.K. Kremer, E. Sigmund, V. Hizhnyakov, F. Hentsch, A. Simon, K.A. Müller and M. Mehring, *Z. Phys. B: Condensed Matter, 86* (1992) 319.
21 S. Kirkpatrick, *Rev. Mod. Phys., 45* (1973) 574.
22 B. Rupp, E. Pörschke, P. Meuffels, P. Fischer and P. Allenspach, *Phys. Rev. B, 40* (1989) 4472.
23 P. Allenspach, A. Furrer and B. Rupp, in V.L. Askenov, N.N. Bogolubov and N.M. Plakida (eds), *Progress in High-Temperature Superconductivity*, Vol. 21, World Scientific, Singapore, 1990, p. 318.
24 B. Roessli, P. Fischer, U. Staub, M. Zolliker and A. Furrer, *Europhys. Lett., 23* (1993) 511.
25 P. Fulde and I. Peschel, *Adv. Phys., 21* (1972) 1.
26 M. Guillaume, U. Staub, F. Fauth, J. Mesot, A. Furrer and C.J. Carlile, *Physica C,* in press.
27 A. Furrer and H. Heer, *Phys. Rev. Lett., 31* (1973) 1350.
28 I.N. Kurkin, I.Kh. Salikhov, L.L. Sedov, M.A. Teplov and R.Sh. Zdanov, *Zh. Eksp. Teor. Fiz., 103* (1992) 1342; *JETP, 76* (1993) 657.
29 U. Staub, P. Allenspach, J. Mesot, A. Furrer, H. Blank and H. Mutka, *Physica B, 180–181* (1992) 417.